Energy Engineering and Management, Vol. 13, No. 4, PP. 26-35, 2024

Examination of PMSM Application in Eelectric Vehicles based on Improved Bi-directional Z Quasi-Source Inverter

Hadi Khorramdel[1], Seyed Reza Mousavi-Aghdam[2*], Farzad Sedaghati[3]

[1] Faculty of Engineering, University of Mohaghegh Ardabili, Ardabil, Iran
hadikhoram.2015@gmail.com
[2] Faculty of Engineering, Energy Management Research Center, University of Mohaghegh Ardabili, Ardabil, Iran
r.mousaviaghdam@uma.ac.ir
[3] Faculty of Engineering, Energy Management Research Center, University of Mohaghegh Ardabili, Ardabil, Iran
farzad.sedaghati@uma.ac.ir

Keywords:
PMSM,
flux attenuation control,
improved Z-source inverter,
DC link voltage regulation,
inverter voltage gain,
input current.

Original Research Article

Paper History:
Received: 09/01/2024
Revised: 06/07/2024
Accepted: 07/07/2024
Available online: 07/07/2024

Abstract: This article proposes a variable permanent magnet drive system with DC link voltage based on an improved impedance quasi-source inverter. The proposed inverter for the permanent magnet drive system has improved compared to the prior inverters used in such a system regarding output voltage gain and input current. In addition to functional analysis and dynamic equations, controller design and realization of an improved bilateral impedance quasi-source inverter for use in electric vehicles are also presented. The circuit analysis shows that with a two-way switch in the impedance pseudo-source network, the performance of the inverter under small inductance and low power factor can be improved. In the flux control method, when there is a disturbance in the input voltage of the circuit, the DC link tends to fluctuate, which is considered a defect. To overcome this problem, a dedicated voltage controller is used to remove the disturbance and stabilize the DC link voltage. A non-connection mode is designed. The simulation results are presented to prove the performance of the circuit and the effectiveness of the proposed control method.

How to cite this article: Khorramdel, H., Mousavi-Aghdam, R., Sedaghati, F., "*Examination of PMSM Application in Eelectric Vehicles based on Improved Bi-directional Z Quasi-Source Inverter*", Energy Engineering and Management, Vol. 13, No. 4, PP. 26-35, 2024. https://doi.org/10.22052/eem.2024.254205.1044

1. Introduction

The development of internal combustion engine vehicles, especially automobiles, is a remarkable achievement of modern technology. Vehicles have played a crucial role in meeting people's transportation needs and have contributed to the progress of society. Unlike other industries, the automobile industry has advanced rapidly, evolving from basic to industrial vehicles. It can be argued that the automotive industry and related sectors are the backbone of the global economy and employ a large portion of the workforce. Besides, electric cars offer numerous advantages over traditional internal combustion engine vehicles such as zero greenhouse gas emissions, high efficiency, reduced dependence on oil and fossil fuels, and quiet smooth operation. The article aims to promote the transition towards clean energy, to decrease fossil energy consumption, and to encourage the use of renewable energy. The engine and control system are crucial components of electric cars. Permanent magnet motors, with their high efficiency and power density, can operate over a wide range of constant torque and achieve superior vehicle performance, especially at high speeds [1]. Voltage source inverters in permanent magnet synchronous motors serve as an interface for electric machines. In this type of inverter, the DC link voltage is supplied by the power source, typically a battery or a large capacitor. When power supply is discharged with a high current, the DC link voltage drops significantly. Conversely, when the power source is charged with a high current, the voltage increases sharply, leading to a decrease in the output power of the motor. These voltage fluctuations impact the control of electric cars. To address this issue, a compromise plan is usually implemented in the motor design to keep the control method from becoming too complex. Achieving this compromise involves adjustments between the number of converter elements and the converter control method to maintain optimal motor performance. However, such changes can increase the motor's size and weight, which is a drawback. To address this, to ensure the stability of the DC link voltage, and to resolve the inconsistency between the power supply voltage and the DC link in permanent magnet synchronous motors, a two-way DC-DC converter is employed. This converter enhances motor torque and widens the motor's operating speed range.

Traditional inverters, such as voltage source inverters, have some issues that affect permanent magnet synchronous motors. To address these problems, researchers have introduced full-bridge and half-bridge impedance source inverters [2, 3]. These inverters can both increase and decrease voltage. They utilize an X-shaped impedance network consisting of two capacitors and two inductors as the interface between the inverter bridge and the DC voltage source. In this type of inverter, the DC link voltage increases when there's a short circuit in the inverter bases, increasing the effective AC load voltage. When the input voltage is high, the converter exits the short-circuit mode, and acts like a buck voltage source inverter. To address the issues with full-bridge and half-bridge impedance source inverters, researchers have developed quasi-impedance source inverters. These inverters directly connect the DC input voltage source and the inductor to produce a continuous input current and suppress the inrush current on the input side. However, the output voltage gain of quasi-impedance source inverters is not improved and remains equal to the traditional impedance source inverter [4]. One of the goals of this research is to enhance the output voltage gain.

Control methods of impedance source inverters have been reviewed in [5, 6]. In addition, modeling, controller design [7-9], and its fields of application [10, 11] have been reviewed in the articles. In [12], an adaptive space vector modulation (SVM) method is presented for a conventional three-level T-NPC inverter to increase the inverter performance over a wide range of speeds in electric vehicles. In a normal impedance source inverter, the voltage stress on the capacitors is very high. Besides, the input current of the source is discontinuous, which is one of the disadvantages of these inverters. To overcome the disadvantages of impedance source inverters, a new impedance source inverter, called embedded impedance source inverter, is presented in [13]. Among the disadvantages of this category of inverters is the lack of a common field between the inverter and the input voltage source; the second disadvantage is the use of two symmetrical sources embedded in the impedance source. In [14], to reduce the nominal value of passive elements in conventional impedance source inverters and to maintain source current continuity, a quasi-impedance source inverter is presented. This structure has many applications in electronic power converters. One of the advantages of this structure is the operation of the converter in short-circuit mode, which happens by adjusting the DC link voltage. The mentioned advantage improves the reliability of the inverter, and this reliability allows the adjustment of the motor speed. Therefore, the design and operation of the pseudo current feed impedance source inverter are proposed in [15]. The DC link voltage of the inverter is adjustable, and the energy consumed when braking the motor is returned to the DC power supply for storage. In [16], the voltage-fed impedance quasi-source inverter is used in the electric drive of the electric vehicle. This paper has analyzed the benefits of the design through simulation. A two-way impedance energy source current converter control system is proposed in [17, 18]. Electrical analysis is also the analysis of electric vehicle motor drive braking systems in this article. The conventional predictive flow control (MPCC) model has the advantages of a simple control structure, fast dynamic response time and easy implementation. However, the MPCC applied to the permanent magnet synchronous motor is very sensitive to the motor parameters, and incorrect model parameters will affect the control performance. Aiming to reduce the sensitivity of the MPCC parameter, a motor parameter-free MPCC method (MPF-MPCC) was proposed in [19]. In [20], the impedance source inverter research was done. Also, in this article, the analysis of the performance and

application of electric cars was stated. The control performance problem of model predictive current control (MPCC) was affected by the accuracy of model parameters, in [21] MPCC permanent magnet synchronous motors (PMSM), based on nonparametric predictive model (NPM-MPCC), were proposed to solve this problem. A quasi-impedance source inverter was used for photovoltaic power generation systems and motor speed control systems [22]. The use of a three-phase impedance source inverter in battery charge and discharge control was proposed in [23]. According to [24], impedance source converters and DC-DC buck-boost converters could adjust the DC link voltage of the inverter. Also, in source-impedance conversion, they should use less active equations, which are considered an advantage. This advantage makes the converter operation in short-circuit mode, and the reliability of the system is also improved [24].

As shown in Fig.1. the pseudo-impedance source converter has the advantages of continuous current and low voltage stress compared to the conventional impedance source converter. A DC link voltage regulator permanent magnet synchronous motor drive system driven by the proposed bidirectional improved inverter. This system is used for traction motor drive systems in electric vehicles to expand the operation range of torque and the speed of permanent magnet synchronous motor and to improve the motor efficiency in high-speed operation areas. In [25], a design method considering overall efficiency optimization for permanent magnet synchronous motor systems for use in electric/hybrid vehicles was proposed. A changeable flux attenuation angle was used in the armature current control method, and the optimal charge attenuation angle for any specific operating condition could be obtained through pre-selection, which improves system efficiency. Then, the optimal LUT (Look Up Table) for the armature current control commands is obtained. By using this optimized.

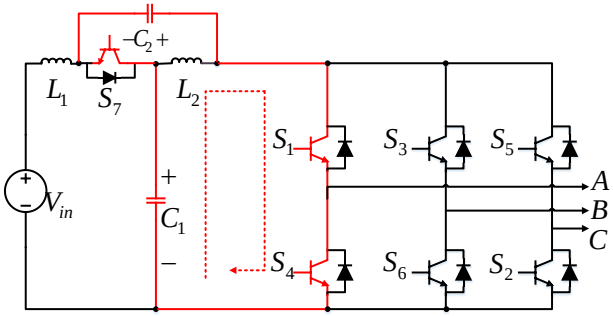

Fig. 1: Impedance quasi-source inverters fed with bidirectional voltage

LUT in the drive system, system efficiency can be significantly improved for the entire operating range. A new control method to transfer the power of a permanent magnet synchronous electric motor with a low safe current limit that discharges the DC link and dissipates the system energy without increasing the DC link voltage is proposed in [26]. A detailed model of the phasor diagram of the permanent magnet synchronous motor as a generator is developed based on the analysis of the different stages of the discharge process. Based on this model, the maximum power discharge method is given the d-axis current, and the q-axis current is received by tracking the location of the current in the paths of voltage limit, current limit, and power limit which have not yet been used in the discharge process. Since this method considers the friction and maximum safe current of the system, the propulsion system discharges the remaining energy at maximum power and reduces the DC link voltage and rotor speed as quickly as possible. According to the load characteristics and special requirements of wind and mooring winches, the design problems, the key points of the permanent magnet motor, and the drive system with low speed and high efficiency are presented in [27]. In this reference, a method for adapting parameters to design a permanent magnet motor with low speed and high efficiency is proposed based on the coupling finite element method. In [28], the permanent magnet synchronous motor is digitally controlled using the classic direct torque control scheme. The use of a permanent magnet synchronous motor drive with direct torque control provides several advantages such as fast and strong torque response, high-performance control speed, and increased efficiency. A systematic method of fault detection and isolation based on structural analysis is presented in [29]. For control purposes in an electric drive system and in an electric car usually different types of sensors are used, including current sensors, voltage sensors, speed sensors, position sensors, and so on in order to be sampled at any moment. The vector felt the changes. In [18], a control method for reducing the energy buffer capacity for a single-phase inverter with an impedance source and pseudo-impedance source is proposed. Also, in [18, 30], the proposed control method is significantly improved without using additional hardware components. It has reduced the need for capacitors. In [31], an experimental implementation of V/f scalar control for a three-phase squirrel cage induction motor is presented. The main purpose of this is to control the speed of rotation set by a reference and maintain it despite the presence of disturbances. To implement the proposed design, two methods have been used, which are: the open loop design, which is usually used in the industry, and the closed loop design which is less used but offers higher performance features. Three-speed control methods for induction motors are shown in [32], one of which is scalar control. In scalar control, the goal is to control the speed by changing the voltage, altering the frequency, and keeping their ratio constant. The second method is the indirect field-oriented control and the last is the direct torque control method. In all these speed control methods, the space vector pulse width modulation method is used for the three-level inverter. Three-level inverters are preferred to reduce voltage stress on switches in medium-voltage drive applications.

According to the mentioned points, the control and proper design of the impedance source converter can have a better effect on the performance of PMSM motors for electric vehicle applications. It can be stated that when operating at base speed, the permanent magnet

synchronous motor is usually controlled by flux weakening methods, which reduces system efficiency. In this paper, a variable PMSM drive system with DC link voltage based on an improved impedance pseudo-source is proposed, and it has improved the system performance. The structure of the article is as follows: in the second part, the analysis of the permanent magnet synchronous motor is discussed. In the third part, the system control design, the introduction of the proposed improved inverter structure, the analysis, and the review followed by the design of the circuit elements are discussed. The fourth section deals with the sensitivity analysis of the proposed improved inverter for different duty cycles. The performance comparison of the proposed structure with other high-gain inverters is described in the fifth section. The sixth section presents the simulation results. Finally, the seventh section concludes this article.

2. Modeling of permanent magnet synchronous motor

In steady state, the equations of d-q axis permanent magnet synchronous motor are as follows:

$$\begin{cases} U_d = Ri_d - \omega L_q i_q \\ U_q = Ri_q + \omega L_d i_d + \omega \psi_f \end{cases} \quad (1)$$

In relation (1), U_d, U_q is the d-q axis voltage, L_d, L_q is the d-q axis inductance, R is the stator resistance, ω is the electrical angular velocity of the motor, and Ψ_f is the permanent magnetic flux link. Considering the limit of inverter voltage and motor winding current, the limit equation of voltage and current can be written as follows:

$$\begin{cases} U^2{}_d + U^2{}_q \le U^2_{\lim} \\ i^2{}_d + i^2{}_q \le i^2_{\lim} \end{cases} \quad (2)$$

$$(L_d i_d + \psi_f)^2 + (L_q i_q)^2 = (U_{\lim} / \omega)^2 \quad (3)$$

In equation (3), it is evident that using the impedance quasi-source inverter can increase U_{lim}. By expanding the radius of the circle, both the voltage limit and the motor rotation speed are heightened, leading to an increase in the motor's torque and speed range. In comparison to the traditional voltage source inverter, it becomes feasible to broaden the speed by weakening the direct axis current flux to enhance the system's efficiency. This is because when the permanent magnet synchronous motor is not operating at high speeds, the loss of the permanent magnet rotor can be disregarded. Additionally, mechanical losses and uncontrollable vortex losses have minimal impacts on the ultimate winding losses of the stator and can, thus, be overlooked. Hence, only the copper and iron losses in the stator winding are factored into the equations. The copper loss due to the motor current in the stator winding resistance can be calculated using the following equation:

$$P_{CU} = \frac{3}{2} R_S (i_d^2 + i_q^2) \quad (4)$$

Based on the iron loss method, the iron loss can be categorized into two types: hysteresis reduction and the eddy current loss. When using a general silicon steel sheet, the hysteresis loss is much higher than eddy current loss at speeds lower than the base speed. At these speeds, the eddy current losses can be disregarded. Therefore, assuming that the total iron loss is almost equal to the hysteresis loss, the permanent magnet synchronous motor's iron loss is obtained as follows:

$$P_{fe} = K_h B^{\beta} P \omega m_{st} \quad (5)$$

In equation (5), k_h represents the hysteresis reduction coefficient, B stands for the magnetic flux density, m_{st} denotes the quality of the stator core, and β is a constant parameter typically falling within the range of 0.2 to 1.8. From the motor's perspective, when utilizing the impedance source inverter, there is no requirement for additional demagnetization current, and copper losses are reduced. Although the basic magnetic flux density decreases due to the implementation of flux reduction, the iron loss remains constant. However, the harmonic iron loss resulting from the armature reaction significantly increases after the adoption of flux reduction, leading to a slight change in the overall iron loss. Compared to flux reduction, the adoption of boost criteria is more advantageous in enhancing motor efficiency. The efficiency of a permanent magnet synchronous motor driven by a boost converter and PWM inverter surpasses the efficiency achieved with flux reduction. Given the above, it is anticipated that the use of an impedance source inverter to boost the DC link voltage and to control all winding current into torque current for improved efficiency is superior to the traditional flux reduction approach. Therefore, this article employs an improved impedance source to boost the DC link voltage.

3. Control System Design

3.1. Introduction of the Proposed Inverter

The proposed inverter configuration is illustrated in Fig. 2. The structure includes two diodes (D_1, D_2), two capacitors (C_1, C_2), seven switches (S, T_C^-, T_C^+, T_B^-, T_B^+, T_A^-, T_A^+), three capacitors (L_1, L_2, L_3), and a voltage source V_{in}. To achieve the ideal gain of the converter, all elements are considered to be lossless. The diode cut-off voltage and the switch and diode losses are disregarded. The capacities are large enough to maintain constant voltage in one cycle, allowing the converter to operate in the D cycle.

3.2. Steady-state Analysis and Voltage Gain

In the first operating mode (0-DT), the inverter bridge is on, and the switches are conducting. In this mode, diodes D_1 and D_2 are on, and the capacitor C_2 is in the circuit. The inverter bridge is driven for an interval of DT when the proposed circuit is in short-circuit mode. D represents the duty cycle, and T is the period of the switching signal. The voltage between two ends of the inductors during the first operating state can be obtained by applying Kirchhoff's voltage law (KVL). In this case, the current of the inductor is increasing, and energy is stored by inductors. Capacitor C1 is charged through D_1, L_2, L_3, D_2, and capacitor C_2 through D_1, L_2. The governing equations for the first mode of operation are in the form of equation (6):

$$\begin{cases} V_{L1} = V_{in} \\ V_{L2} + V_{L3} = V_{C1} - V_{C2} \\ \dfrac{di_{L1}}{dt} = \dfrac{V_{in}}{L_1} \\ \dfrac{di_{L2}}{dt} = \dfrac{V_{C1}}{L_2}, \dfrac{di_{L3}}{dt} = \dfrac{V_{C1}}{L_3} \\ I_{C1} = I_{L1} \\ I_{C2} = I_{L2} \\ I_{C3} = I_{L2} \end{cases} \quad (6)$$

In the second mode of operation, the S switch is conducting while the diodes D_1 and D_2 are reverse-biased. During this functional state, the energy stored in the second and third inductors is discharged into the load and the first capacitor. This action causes the load to start and charge the capacitor. The capacitor C_1 is charged by the input source and the first inductor. The relationships related to this functional state can be expressed in the form of equation (7):

$$\begin{cases} V_{L1} = V_{in} - V_{c1} \\ V_{L2} + V_{L3} = V_{C1} - V_O \\ V_{L2} = \dfrac{2V_{C1} - V_O}{2} \\ \dfrac{di_{L1}}{dt} = \dfrac{V_{in} - V_{C1}}{L_1} \\ \dfrac{di_{L2}}{dt} = \dfrac{2V_{C1} - V_O}{L_2} \\ \dfrac{di_{L3}}{dt} = \dfrac{2V_{C1} - V_O}{L_3} \\ I_{L1} = -I_{C2} - I_o \\ I_{L2} = I_{L3} = I_{C1} - I_o \end{cases} \quad (7)$$

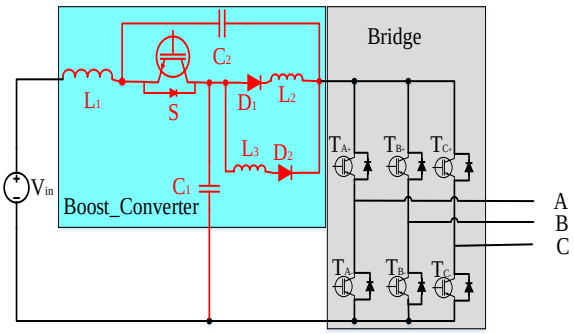

Fig. 2: Configuration of the proposed inverter

By applying the principle of volt-second balance on L_1 inductors and using KVL, the voltage of the two ends of the first capacitor is obtained as follows:

$$\begin{cases} V_{C1} = V_{C2} = \dfrac{V_{in}}{1-D} \\ V_S = \dfrac{2V_{in}}{(1-D)^2} \end{cases} \quad (8)$$

By applying the volt-second balance principle in inductor L_2 and substituting the value of V_{C1} from equation (8), the converter gain value is obtained as:

$$V_O = \frac{2V_{in}}{(1-D)^2} \quad (9)$$

3.3. Active Switch Control (S)

To prevent abnormal operation conditions and to ensure that the proposed inverter can handle a wide range of load changes, an anti-parallel switch S is used on the input side of the converter. During one cycle of the switching method, the S switch complements the short-circuit pattern of the three-phase bridge. When the three-phase bridge is in the short-circuit state, the S switch conducts, and the diode connected to S is off. This operation of the switch increases the circuit voltage because when the three-phase bridge is in the short-circuit state, the switch S is closed, and the reverse current passes through the switch, causing energy to return to the DC source (braking mode). To avoid circuit damage and ensure the safety of the proposed converter, a suitable dead time should be included between the control signals in the short-circuit mode and the conduction of the S switch. Otherwise, the capacitor and diode in the converter may be short-circuited through the S switch, causing damage to the circuit.

The proposed method for generating switching pulses which uses a converter is illustrated in Fig. 3. To create the switch pulse, three triangular waveforms with a phase difference and two carrier signals are employed to achieve the short circuit mode. As depicted in Fig. 3. both V_P and V_N signals serve as short-circuit references for the proposed structure. When the carrier signal surpasses V_P, it results in a high reference and high coverage, whereas it leads to a low reference and low coverage if it surpasses V_N. When the three-phase reference signals (V_a, V_b, V_c) meet one of the short-circuit conditions, the gate signals for the active mode and zero mode are identical to those of the traditional SPWM method. The only difference is that there is only one short-circuited state for the zero state. The short-circuit control is a straight line that is equal to or higher than the upper envelope of the modulation waves or equal to or less than the lower envelope of the modulation waves. Consequently, the maximum short-circuit ratio can be calculated as (1-M). It is apparent that as the modulation index increases, the parameter M decreases, resulting in the short-circuit ratio approaching zero. Conversely, as the parameter M equals one, the inverter functions as a traditional voltage source inverter.

3.4. Switching method Design

In this article, Fig. 3, demonstrates the use of the PWM switching method to control the S_1-S_6 switches to enhance the performance of the converter. The aim is to simplify the control structure, to increase the efficiency of the voltage generated by the DC link, and to reduce the induced current. The upper bridge and lower bridge switches are distinguished by the "+" and "-" subscripts. The symbols T_A^+, T_B^+, T_C^+, T_A^-, T_B^-, and T_C^- are used to indicate the switching time and the moment of turning off and turning on the switches in the proposed inverter bridge structure. Additionally, incorporating dead time in the control of the switches is necessary to improve the reliability of the converter.

3.5. Developing a General Control Method

In the control method described for the proposed structure, Fig. 4, shows that the inductor current L_1 is utilized as the inner loop and the capacitor voltage C_1 is utilized as the outer loop. Controlling the capacitor voltage is essential to regulate the DC link voltage, which in turn increases the current. To prevent this, the inductor current, serving as the inner loop, is utilized to counteract the current increase, thus improving the system's dynamic response.

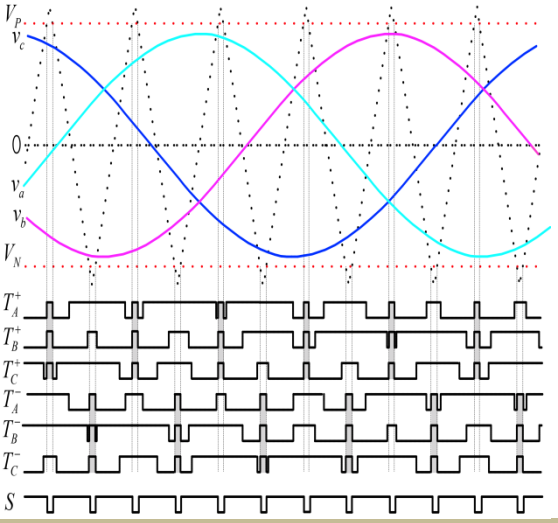

Fig. 3: Switching method and how to guide the keys to generate pulses

When the DC link voltage is set using real-time methods, the DC link voltage command is defined as follows:

$$V_{dc}^{*} = \omega\sqrt{3*(L_d i_d + \psi_f)^2 + (L_q i_q)^2} \qquad (10)$$

3.6. Design of the Proposed Inverter Elements

According to the analysis of the stability state of the proposed inverter in the previous section, by integrating equations (6) and (8), we can obtain the current ripple (i_{L1}, i_{L2}, i_{L3}) and voltage waves (C_1 and C_2).

$$\begin{cases} \Delta i_{L1} = \dfrac{DV_i}{L_1 f_S} \\ \Delta i_{L2} = \dfrac{DV_i}{L_2 f_S} \\ \Delta i_{L3} = \dfrac{DV_i}{L_3 f_S} \end{cases} \qquad \begin{cases} \Delta V_{C1} = \dfrac{2MDV_i}{2(1-D)^2 RC_1 f_S} \\ \Delta V_{C2} = \dfrac{2MDV_i}{2(1-D)^2 RC_2 f_S} \end{cases} \qquad \text{M=1-D} \qquad (11)$$

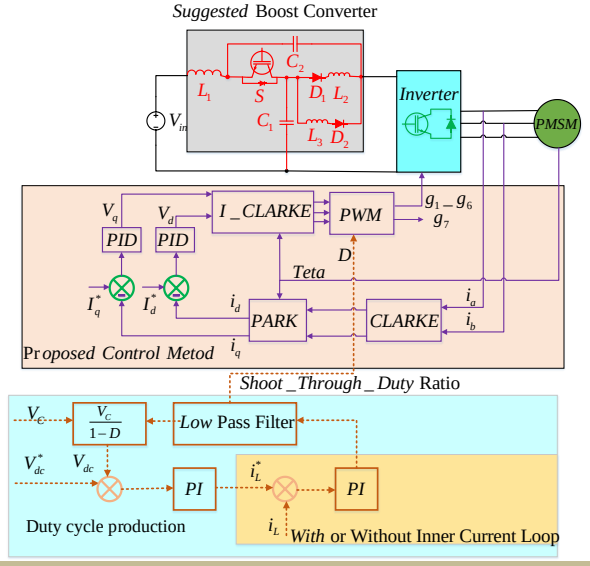

Fig. 4: Control of the proposed structure of the permanent magnet synchronous motor system

Based on equation (10), a safety margin should be considered in the control implementation of the proposed structure. Detailed calculations and controller design are described in reference [1].

4. Sensitivity Analysis (Simulation Results and Mathematical Analysis for Different Operational Cycles)

In this section, the results of simulation and mathematical analysis for different cycles are provided. The parameters of the simulation results are listed in Table 2.

4.1. Proposed Converter Modeling for 0.3 Duty Cycle

Fig. 5 displays the output voltage waveform of phase A with a peak value of approximately 892 volts. According to equation (9), the output voltage value is 897 volts at a 0.3 duty cycle, which aligns with the simulation results. In Fig. 6, the peak voltage for the first capacitor is 310 volts. As per equation (8), the first capacitor's voltage at 0.3 cycles is 314 volts, further supported by the simulation results. Figure (7) depicts the voltage waveform of the second capacitor with a peak voltage of about 310 volts, which matches the calculated 314 volts at the 0.3 duty cycle according to equation (8) and the confirming simulation results.

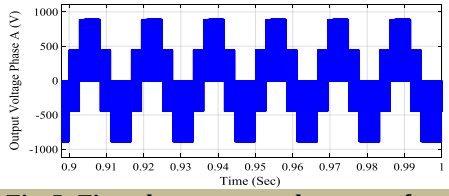

Fig. 5: First phase output voltage waveform

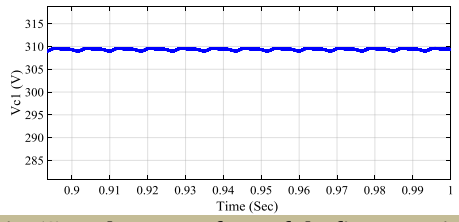

Fig. (6): Voltage waveform of the first capacitor

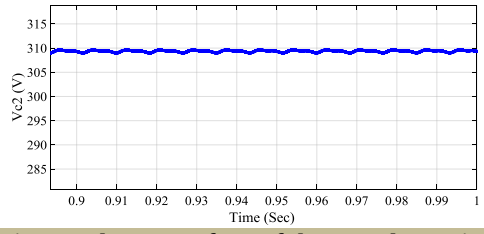

Fig. 7: Voltage waveform of the second capacitor

5. Comparison of the Proposed Converter with the Introduced Converters

In Fig. 8, the gain of the proposed structure is compared with the voltage gain of the impedance source inverter and the prior pseudo-impedance source inverter. The figure shows that the efficiency of the proposed structure is higher than prior inverters such as impedance source inverters, impedance quasi-source inverters, voltage source inverters, and current source inverters. Another advantage of the proposed structure is its wide sensitivity range, which exceeds similar structures prior and makes it suitable for various applications. This converter also offers advantages such as reduced input current ripple and lower voltage stress on the elements compared to prior designs. In Fig. 9, the comparison of the voltage stress on the proposed inverter capacitor is shown about prior similar structures. However, a disadvantage of the proposed structure is the high number of inactive elements. This is due to the better gain factor of the proposed structure, which results in higher voltage at both ends of the switches. Additional notes and comparisons are detailed in Table 1.

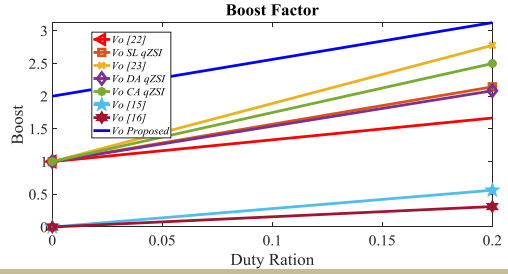

Fig. 8: Comparison of the proposed inverter gain with prior inverters in terms of duty cycle

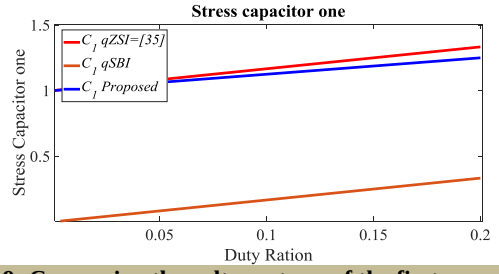

Fig. 9: Comparing the voltage stress of the first capacitor

Table 1: Comparison of the proposed structure in terms of voltage stress of the switch, capacitor, and gain with the prior structures

Suggested	[35]	qSBI	qZSI	
$\begin{cases} V_{C1}=\frac{V_{in}}{1-D} \\ V_{C2}=\frac{V_{in}}{1-D} \end{cases}$	$V_{C1}=\frac{1-D}{1-2D}V_{in}$	$V_{C1}=\frac{D}{1-2D}V_{in}$	$\begin{cases} V_{C1}=\frac{1-D}{1-2D}V_{in} \\ V_{C2}=\frac{D}{1-2D}V_{in} \end{cases}$	V_c
$V_S=\frac{2V_{in}}{(1-D)^2}$	$V_S=\frac{V_{in}}{(1-2D)}$	$V_S=\frac{V_{in}}{(1-2D)}$	$V_S=\frac{V_{in}}{(1-2D)}$	V_s
$B=\frac{2V_{in}}{(1-D)^2}$	$B=\frac{1}{1-2D}$	$B=\frac{1}{1-2D}$	$B=\frac{1}{1-2D}$	B

6. Simulation Results

In this section, simulation results are presented to validate the bidirectional power flow and evaluate the effectiveness of the proposed control approach for the specified inverter. The simulation was conducted in the Simulink MATLAB environment.

The elements' sizes used in the proposed converter are listed in Table 2. The DC input power supply of the 220V inverter is chosen to provide the required voltage for the traction drive, and the drive can generate the energy needed to operate an induction motor. The PWM carrier frequency is set at 10 kHz. Because the short circuit mode is divided equally into two parts in one switching period, the switching frequency for the S switch is 20 kHz. Simulations were carried out to demonstrate the superiority of the inverter structure in terms of gain and element stress compared to prior structures to match the analysis results with the simulation results and to prove the necessity and effectiveness of the control loop; thereby, they confirm the effectiveness of this control method to validate the proposed structure. Fig. 10 depicts the input current of the proposed converter, which is continuous due to the presence of the inductor, resulting in fewer ripples. Fig. 11 shows the waveform of the DC link voltage with a duty cycle of 0.28 at the input voltage of 220 volts. According to the mathematical analytical relation (9), the DC link voltage should be 848 volts, confirming the simulation results of the mathematical analysis. The slight difference is due to the ideal consideration of all elements in the analysis:

$$\begin{cases} V_o=\frac{2}{(1-D)^2}V_{in} \\ V_{in}=220V \quad \Rightarrow V_o=848V \\ D=0.28 \end{cases} \tag{11}$$

Table 2: The size of the elements used and the parameters of the motor in the structure

Inductor (L_1 , L_2, L_3)	500 µH
Capacitors (C_1, C_2)	840 µF
Frequency	50HZ
Switch	IGBT
Number Phase PMSM	3
Rotor Type	Round
Mechanical Input	Torque Tm
Preset Model	02:1.7Nm 300V_{dc} 3750 RPM_1.7 Nm
Stator Phase Resistance R_s	4.765 ohm
Armature Inductance	0.014 H
Flux Linkage	0.1848

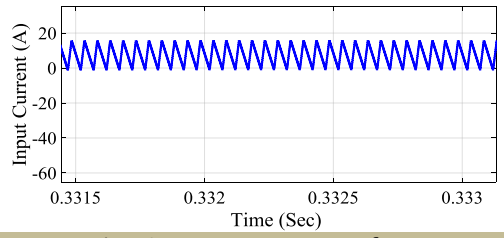

Fig. 10: Input current waveform

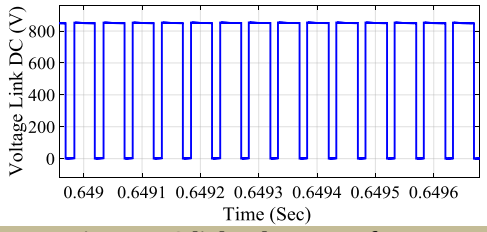

Fig. 11: DC link voltage waveform

Fig. 12 shows the waveform of the first capacitor for the proposed converter. According to equation (12), according to the mathematical analysis, the voltage value of the first capacitor is equal to 306 volts, which proves the simulation results of the mathematical analysis.

$$\begin{cases} V_{C1} = \dfrac{V_{in}}{1-D} \\ V_{in} = 220V \Rightarrow V_{C1} = 306V \\ D = 0.28 \end{cases} \quad (12)$$

In Fig. 12, the capacitor voltage ripple shows less fluctuation in the stable state. Fig. 13 displays the waveform of the second capacitor for the proposed converter. Based on equation (13) and mathematical analysis, the voltage value of the second capacitor is determined to be 306 volts, which aligns with the simulation results.

$$\begin{cases} V_{C2} = \dfrac{V_{in}}{1-D} \\ V_{in} = 220V \Rightarrow V_{C2} = 306V \\ D = 0.28 \end{cases} \quad (13)$$

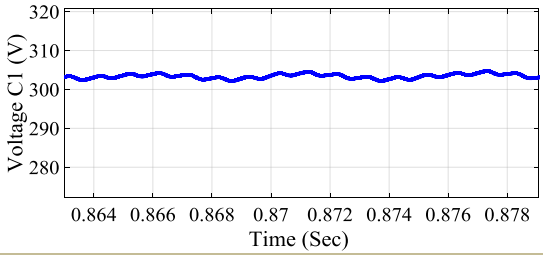

Fig. 12: Voltage waveform of the first capacitor

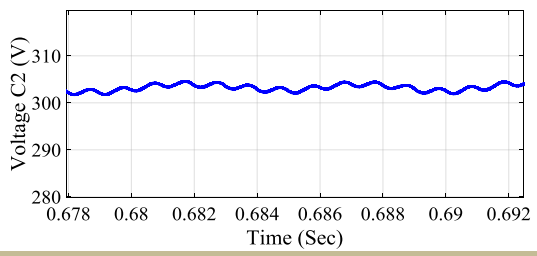

Fig. 13: Voltage waveform of the second capacitor

In Fig. 14, the waveform of the first inductor for the proposed converter is shown. Based on the mathematical analysis in equation (14), it is determined that the voltage across the first inductor is 220 volts, confirming the simulation results.

$$\begin{cases} V_{L1} = V_{in} \\ V_{in} = 220V \end{cases} \Rightarrow V_{L1} = 220V \quad (14)$$

The voltage waveform of the inverter bridge switches, illustrated in Fig. 15, appears as a square pulse. The maximum voltage applied to the switches is uniform, ensuring equal lifespan and power distribution. As per equation (15) and mathematical analysis, the voltage across the switches measures 848 volts, corroborating the simulation results.

$$\begin{cases} V_S = B = \dfrac{2V_{in}}{(1-D)^2} \\ V_{in} = 220V \\ D = 0.28 \end{cases} \Rightarrow V_S = 848V \quad (15)$$

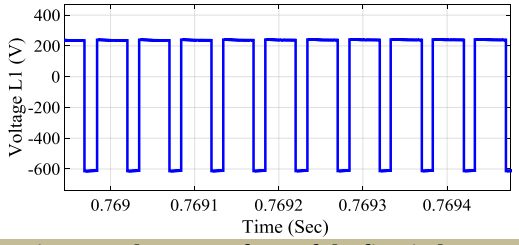

Fig. 14: Voltage waveform of the first inductor

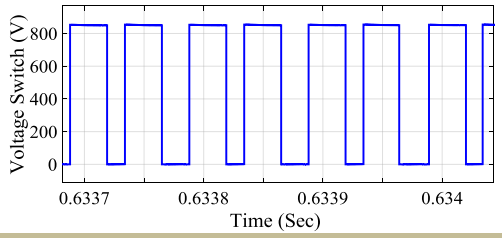

Fig. 15: Voltage waveform of inverter bridge switches

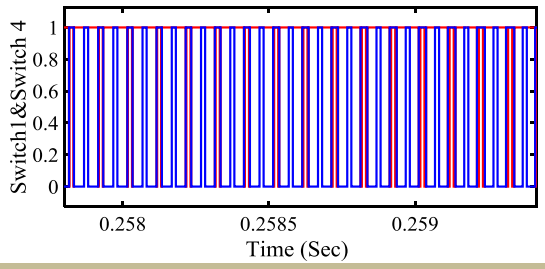

Fig. 16: The pulsing waveforms of the first and fourth switches

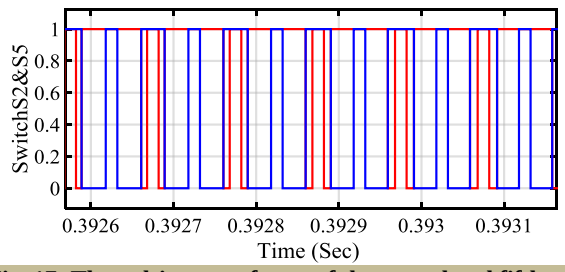

Fig. 17: The pulsing waveforms of the second and fifth switches

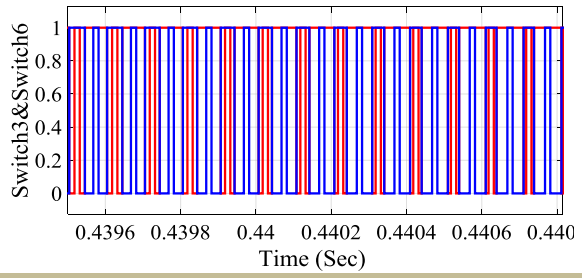

Fig. 18: The pulsing waveforms of the third and sixth switches

Fig. 16, 17, and 18 illustrate how to pulse the Switches of one leg of the inverter bridge. In the event of a short circuit, the switches of one leg cannot be turned on or off simultaneously. Therefore, in an inverter bridge, the upper and lower switches operate in opposite phases.

Fig. 19 displays the motor stator current waveform, showing that the three-phase current has a sinusoidal waveform with a low total harmonic distortion (THD) value. This results in a sinusoidal output waveform, minimizing losses on the stator.

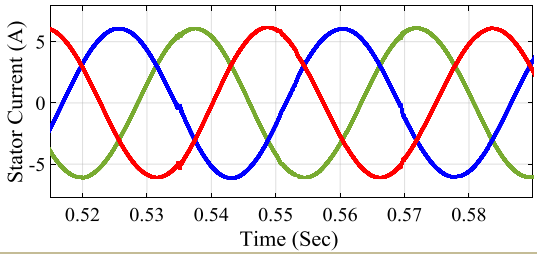

Fig. 19: Stator current waveform

Fig. 20 illustrates the voltage waveform of the DC link control switch, which takes the form of a square pulse. The maximum voltage applied to this switch is the same as that of the inverter bridge switches.

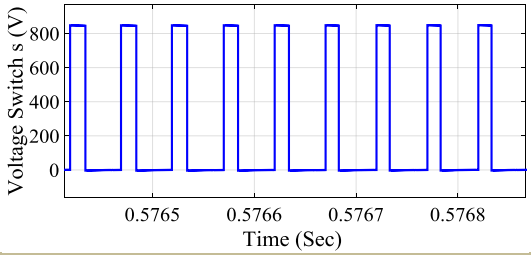

Fig. 20: S key voltage waveform

Fig. 21 showcases the waveform of the rotor speed and electromagnetic torque when receiving energy. Additionally, this figure demonstrates the system's robustness in terms of dynamics and confirms the stability of the proposed converter for permanent synchronous motors, which also includes tracking capability.

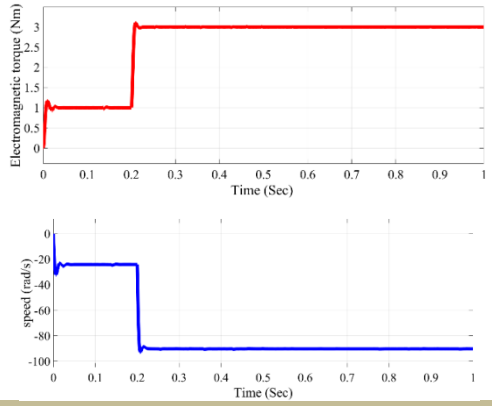

Fig. 21: waveform of rotor speed and torque

7. Conclusion

This article presents the design of a DC link voltage-regulated permanent magnet synchronous motor drive system. The system is based on an improved impedance pseudo-source and is fed with a voltage source. The control method used for this system is an internal and external double loop. In the proposed inverter control, the inductor current forms the inner loop, while the capacitor voltage on the inverter side is the source of the improved impedance, forming the outer loop. The simulation results demonstrate that the proposed system exhibits good dynamic stability. Additionally, the converter shows an acceptable voltage gain value and a continuous input current with minimum ripple. The use of the improved impedance quasi-source inverter to increase the link voltage has been shown to expand the speed range and torque of the motor. The control method and the nature of the proposed inverter have significantly improved the operation range of the motor and the system efficiency in comparison to prior methods, including the traditional method of flux weakening.

References

[1] Wang, R., Jia, X., Dong, S., Zhang, Q., "*PMSM driving system design for electric vehicle applications based on bi-directional quasi-Z-source inverter*", 13th IEEE Conference on Industrial Electronics and Applications (ICIEA) IEEE., pp. 1733-1738, 2018.

[2] Peng, F. Z., "*Z-source inverter*", IEEE Transactions on industry applications, Vol. 39, No. 2, pp.504-510, 2003.

[3] Babaei, E., Asl, E. S., "*High voltage gain halfbridge Z-source inverter with low voltage stress on capacitors*", IEEE Trans., Vol. 64, No. 1, pp. 191–197, 2017.

[4] Zhu, X., Ye, K., Jiang, L., Jin, K., Zhou, W., Zhang, B., "*Nonisolated single-phase quadratic switched-boost inverter with continuous input current and step-up inversion capability*", IEEE Journal of Emerging and Selected Topics in Industrial Electronics, Vol. 4, No, 1, pp. 276-287, 2023.

[5] Tran, Q. V., Chun, T. W., Ahn, J. R., Lee, H. H., "*Algorithms for controlling both the dc boost and ac output voltage of Zsource inverter*", IEEE Trans, Vol. 54, No. 5, pp. 2745–2750, 2007.

[6] Asl, E. S., Babaei, E., Sabahi, M., Nozadian, M. H. B., Cecati, C., "*New half-bridge and fullbridge topologies for a switched-boost inverter with continuous input current*", IEEE Trans, Vol. 65, No. 4, pp. 3188-3197, 2018.

[7] Peng, F.Z., Joseph, A., Wang, J., Shen, M., Chen, L., Pan, Z., Ortiz-Rivera, E., Huang, Y., "*Z-source inverter for*

motor drives", IEEE Trans. Power Electron., Vol. 20, No. 4, pp. 857–863, 2005.

[8] Peng, F.Z., Shen, M., Holland, K., "*Application of Zsource inverter for traction drive of fuel cell-battery hybrid electric vehicles*", IEEE Trans. Power Electron., Vol. 22, No. 3, pp. 1054–1061, 2007.

[9] Huang, Y., Shen, M., Peng, F.Z., Wang, J., "*Z-source inverter for residential photovoltaic systems*", IEEE Trans. Power Electron., Vol. 21, No. 6, pp. 1776–1782, 2006.

[10] Loh, P.C., Vilathgamuwa, D.M., Gajanayake, G.J., Lim, Y.R., Teo, C.W., "*Transient modeling and analysis of pulse-width modulated Z-source inverter*", IEEE Trans. Power Electron., Vol. 22, No. 2, pp. 498–507, 2007.

[11] Liu, J.B., Hu, J.G., Xu, L.Y., "*Dynamic modeling and analysis of Z-source converter-derivation of ac small signal model and design-oriented analysis*", IEEE Trans. Power Electron., Vol. 22, No. 5, pp. 1786–1796, 2007.

[12] Jelodar, Y. J., Salari, O., Youssef, M. Z., Ebrahimi, J., Bakhshai, A., "*A Novel Control Scheme for Traction Inverters in Electric Vehicles With an Optimal Efficiency Across the Entire Speed Range*", IEEE Access., Vol. 12, pp. 25906-25916, 2024.

[13] Gao, F., Loh, P.C., Li, D., Blaabjerg, F., "*Asymmetrical and symmetrical embedded Z-source inverters*", IET Power Electron., Vol. 4, No. 2, pp. 181– 193, 2011.

[14] Anderson, J., Peng, F.Z., "*Four quasi-Z-source inverters*", IEEE Power Electronics Specialists Conference IEEE., pp. 2743-2749, 2008.

[15] Yang, S., Peng, F. Z., Lei, Q., Inoshita, R., Qian, Z., "*Current-fed quasi-Z-source inverter with voltage Buck–Boost and regeneration capability*", IEEE Transaction., Vol. 47, No. 2, pp. 882-892, 2010.

[16] Guo, F., Fu, L., Lin, C. H., Li, C., Choi, W., Wang, J., "*Development of an 85-kW bidirectional quasi-Z-source inverter with DC-link feed-forward compensation for electric vehicle applications*", IEEE Transactions on Power Electronics., Vol. 28, No. 12, pp. 5477-5488, 2013.

[17] Ahmad, J., Zaid, M., Sarwar, A., Tariq, M., Sarwer, Z., "*A new transformerless quadratic boost converter with high voltage gain*", Smart Science, Vol 8, No. 3 , pp. 163-183, 2020.

[18] Zhou, Y., Li, H., Li, H., "*A single-phase PV quasi-Z-source inverter with reduced capacitance using modified modulation and double-frequency ripple suppression control*", IEEE Transactions on Power Electronics, Vol. 31, No. 3, pp.2166-2173, 2015.

[19] Zhang, X., Zhang, C., Wang, Z., Rodríguez, J., "*Motor-Parameter-Free Model Predictive Current Control for PMSM Drives*", IEEE Transactions on Industrial Electronics., Vol. 71, No. 6, pp. 5443-5452, 2023.

[20] Liu, P., Liu, H. P., "*Permanent-magnet synchronous motor drive system for electric vehicles using bidirectional Z-source inverter*", IET Electrical Systems, Vol. 2, No. 4 ,pp. 178-185, 2012.

[21] Zhang, X., Liu, Z., Zhang, P., Zhang, Y., "*Model Predictive Current Control for PMSM Drives Based on Nonparametric Prediction Model*", IEEE Transactions on Transportation Electrification, Vol. 10, No. 1 , pp. 711-719, 2024.

[22] Jie, L., Baoming, G., Liwen, Z., "*Modeling and Control of the Quasi-Z-source Inverter*", Electric Drive, Vol. 40, No. 4, pp. 36-40, 2010.

[23] Xing, Z., Xinquan, T., Shuying, Y., "*Study on the Three-phase Reversible Z-source Converter for Battery Charge-discharge System [J]*", Power Electronics. Vol. 06, pp. 18-20, 2009.

[24] Xiao, S., Shi, T., Li, X., Wang, Z., Xia, C., "*Single-current-sensor control for PMSM driven by quasi-Z-source inverter*", IEEE Transactions on Power Electronics, Vol. 34, No. 7, pp. 7013-7024, 2018.

[25] Wu, J., Wang, J., Gan, C., Sun, Q., Kong, W., "*Efficiency optimization of PMSM drives using field-circuit coupled FEM for EV/HEV applications*", IEEE Access, Vol. 6, pp. 15192-15201, 2018.

[26]Yang, H., Yang, J., Zhang, X., "*DC-bus capacitor maximum power discharge strategy for EV-PMSM drive system with small safe current*", IEEE Access. Vol. 9, pp. 132158-132167, 2021.

[27] Zhou, G. H., Qiao, M. Z., Zhang, X. F., Xie, J. H., Hao, Q. L., Wan, C., Zhou, Y., "*Development of a low-[14] speed high-efficiency PMSM and its drive system for electric windlass and mooring winch*", IEEE Access, Vol. 10, pp. 70620-70629, 2022.

[28] Morales-Caporal, R., Leal-López, M. E., de Jesús Rangel-Magdaleno, J., Sandre-Hernández, O., Cruz-Vega, I., "*Direct torque control of a PMSM-drive for electric vehicle applications*", In 2018 International Conference on Electronics, Communications and Computers (CONIELECOMP), pp. 232-237. IEEE, 2018.

[29] Zhang, J., Yao, H., Rizzoni, G., "*Fault diagnosis for electric drive systems of electrified vehicles based on structural analysis*", IEEE Transactions on Vehicular Technology, Vol. 66, No. 2, pp. 1027-1039, 2016.

[30] ARULDASS, R., HIMABINDU, S., KUMAR, Y. V., "*A Three-Phase PV Quasi-Z-Source Inverter with Reduced Capacitance Using Modified Modulation and Double-Frequency Ripple Suppression Control*", International Jornal of Scientific Engineereering and Technology Research, Vol. 06, No. 15, pp. 2842-2849, 2017.

[31] Peña, J. M., Díaz, E. V., "*Implementation of V/f scalar control for speed regulation of a three-phase induction motor*", In 2016 IEEE ANDESCON, pp. 1-4, 2016.

[32] Sadhwani, R., Ragavan, K., "*A comparative study of speed control methods for induction motor fed by three level inverter*", In *2016 IEEE 1st International Conference on Power Electronics, Intelligent Control and Energy Systems* (ICPEICES), pp. 1-6, 2016.

[33] Ding, S., Wang, F., "*A new negative output buck–boost converter with wide conversion ratio*", IEEE Trans. Ind. Electron., Vol. 64, No. 12, pp. 9322–9333, 2017.

[34] Mayo-Maldonado, J. C., Valdez-Resendiz, J. E., Garcia-Vite, P. M., Rosas-Caro, J. C., del Rosario Rivera-Espinosa, M., Valderrabano-Gonzalez, A., "*Quadratic buck–boost converter with zero output voltage ripple at a selectable operating point*", IEEE Transactions on Industry Applications, Vol. 55, No. 3, pp. 2813–2822, 2019.

[35] Nguyen, M. K., Tran, T. T., "*A single-phase single-stage switched-boost inverter with four switches*", IEEE Transactions on Power Electronics, Vol.33, No. 8, pp.6769-6781, 2018.